Control of epileptiform spikes based on nonlinear unscented Kalman filter*

Liu Xian(刘 仙)†, Gao Qing(高 庆), and Li Xiao-Li(李小俚)

Key Lab of Industrial Computer Control Engineering of Hebei Province, Institute of Electrical Engineering, Yanshan University, Qinhuangdao 066004, *China*

(Received 4 March 2013; revised manuscript received 7 June 2013; published 19 November 2013)

A new control strategy based on nonlinear unscented Kalman filter (UKF) is proposed for a neural mass model that serves as a model for simulating real epileptiform stereo-electroencephalographic (SEEG) signals. The UKF is used as an observer to estimate the state from the noisy measurement because it has been proved to be effective for state estimation of nonlinear systems. A UKF controller is constructed via the estimated state and is illustrated to be effective for epileptiform spikes suppression of aforementioned model by numerical simulations.

Keywords: unscented Kalman filter (UKF) control, epileptiform spike, closed-loop control, neural mass model

PACS: 02.30.Yy, 87.19.le **DOI:** 10.1088/1674-1056/23/1/010202

1. Introduction

Electroencephalography (EEG) signal plays a significant role in brain research,[1,2] most notably in the diagnosis and classification of neurological diseases such as epilepsy,[3] schizophrenia,[4] and parkinson.[5] Modeling of EEG signals is therefore especially useful for the mechanism analysis of neurological diseases. It is very hard to model real network dynamics at the neural level because the categories of neurons are manifold and the connections of neurons are complex. Since the 1970s the neural mass models have been the preferred models to produce EEG signal.[6] These models describe the activity of neurons at the macroscopic level, i.e., the activity of populations of neurons. They originate from the seminal work of Lopes Da Silva *et al.*[7] for alpha rhythms generation. Recently, they have been applied to account for more complex transient and oscillatory behavior.[8]

At the onset of neurological diseases, EEG signal exhibits specific characteristics. For example, EEG recordings during epileptic seizures often have abnormally large-amplitude rhythmic patterns called spikes. An substantial progress in the use of neural mass models is to simulate the dynamics of real EEG signals measured in the hippocampus during the transition from interical to fast ictal activity of epilepsy seizures.[9] An epileptic neural mass exhibits features of excitability which is reflected in its use to produce inter-ictal spiking activities in a single population in response to random input.[9,10] Studies also show that spiking activity can be propagated between populations in networks of two and three coupled neural populations.[9] More recently, neural mass models containing two explicitly modeling time scales of inhibition are provided by Goodfellow *et al*. to produce slow spike-wave discharges as well as sinusoidal background oscillations, thus providing the method for a parameter driven transition to epilepsy seizure.[11] The effect of local functional heterogeneities which are considered crucial for the mechanisms of epilepsy[12] is investigated in a spatially extended neural mass formulation with local excitatory and inhibitory circuits.[13] These investigations play important roles in understanding the mechanisms of epilepsy seizures.

However, until now clinical electrotherapy for seizures relies heavily on empirical tuning of parameters and protocols,[14,15] the effects of which are usually not optimal. Recently, it has been reported that the closed-loop control via feedback can optimize the entire seizure control process including efficacy of treatment, minimization of side effects, improvement of response by providing intermittent or minimal stimulation, reduction of damage, and minimization of power consumption.[16] In the closed-loop control strategy, control effects are evidently state-specific. Thus, the development of feedback algorithms requires precise metric of system state. The classical circle criterion is applied to construct a robust observer for the state estimation of neural mass models.[17] Kalman filter (KF) together with extended Kalman filter (EKF) and unscented Kalman filter (UKF) is a promising powerful tool for estimating states of dynamical systems. It forms an important component of model-based predictive control. KF is applicable to linear systems in communication and control with a statistical nature for predicting random signals or separating random signals from random noise.[18] EKF faces the difficulties arising from the bias introduced by truncation of the Taylor series expansion of the nonlinear equations of the underlined system and the estimation of deriva-

*Project supported by the National Natural Science Foundation of China (Grant Nos. 61004050 and 60125019) and the Natural Science Foundation of Scientific Research of Hebei Education Department, China (Grant No. 2009482).

†Corresponding author. E-mail: liuxian@ysu.edu.cn

© 2014 Chinese Physical Society and IOP Publishing Ltd

tives from data observations.[19] It is not feasible at all for non-differentiable systems. UKF allows the recursive estimation of system state for nonlinear systems.[20–23] It approximates a posteriori probability density of the estimated state by a Gaussian distribution and propagates the mean and covariance of the estimated state by specifying an ensemble of points (sigma points) that characterize the state. In comparison with the EKF, the UKF requires no computation of derivatives in linearizing nonlinear systems and no truncation of the nonlinear function from linearization. Consequently, such a strategy proves more accurate than the EKF and is especially applicable to the estimation of nonlinear systems. Recently, the application of UKF to observe state and track dynamics from a spatiotemporal computational model of cortical dynamics[24] and Hodgkin–Huxley equations[25] has been demonstrated. In this work, a closed-loop control strategy based on the UKF is proposed to control epileptiform spikes in a neural mass model. The UKF plays a role of observing the system state. Numerical results are given to demonstrate the effectiveness of the proposed UKF control strategy.

2. The neural mass model

The neural mass model is illustrated in Fig. 1. Figure 1(a) shows a single neural population model, where a cluster of neurons is classified into two subsets. Subset 1 represents pyramidal cells that receive excitatory and inhibitory feedback from subset 2. It is characterized by two dynamic linear transfer functions which change the average pulse density of action potentials into excitatory and inhibitory post-synaptic membrane potentials, EPSP or IPSP, respectively, and by a static nonlinear function that relates the average membrane potential of a given subset into an average pulse density of potentials fired by the neurons. The impulse response of the linear transfer function is given by

$$h_{e1}(t) = w(t)Aat\,e^{-at} \tag{1}$$

for the excitatory case and

$$h_i(t) = w(t)Bbt\,e^{-bt} \tag{2}$$

for the inhibitory case, where $w(t)$ is the Heaviside function, A and B are average excitatory and inhibitory synaptic gains which determine the maximal amplitude of the postsynaptic potentials, a and b are connected to both the membrane average time constant and the average distributed time delays in the dendritic tree. If time constants $1/a$ and $1/b$ are fixed, A and B can be applied to adjust the sensitivity of excitatory and inhibitory synaptic, respectively. The static nonlinear function is formulated as the sigmoid function

$$S(v) = \frac{2e_0}{1+e^{r(v_0-v)}}, \tag{3}$$

where $2e_0$ is the maximum firing rate, v_0 is the postsynaptic potential corresponding to a firing rate e_0, and r is the steepness of the sigmoid. Subset 2 is composed of interneurons (non-pyramidal cells, stellate or basket cells) that only receive excitatory input. It is modeled in a similar way, but only one linear transfer function is necessary since input to interneurons is excitatory. The impulse response of the linear transfer function is given by

$$h_{e2}(t) = w(t)Aat\,e^{-at}. \tag{4}$$

In addition, an excitatory input $p(t)$ is used to model the influence of neighboring or distant populations on subset 2. It globally represents the average density of afferent action potentials. Interactions between pyramidal cells and interneurons are summarized by four connectivity constants $C_1 - C_4$, which account for the intrinsic circuitry and the average number of synaptic contacts. By using Laplace transformation, equations (1), (2), and (4) can be represented by second-order ordinary differential equations with the following unified form:

$$\ddot{z}(t) = Ggx(t) - 2g\dot{z}(t) - g^2 z(t), \tag{5}$$

where $G = A$ and $g = a$ for $h_{e1}(t)$ and $h_{e2}(t)$, $G = B$ and $g = b$ for $h_i(t)$, $x(t)$ and $z(t)$ are the input and output signals. By introducing a new variable $z_1(t)$ and letting $\dot{z}(t) = z_1(t)$, equation (5) can also be written as follows:

$$\begin{cases} \dot{z}(t) = z_1(t), \\ \dot{z}_1(t) = Ggx(t) - 2gz_1(t) - g^2 z(t). \end{cases} \tag{6}$$

Thus, the single neural population model given in Fig. 1(a) is governed by the following set of six first-order ordinary differential equations:

$$\begin{cases} \dot{x}_1(t) = x_2(t), \\ \dot{x}_2(t) = AaS[x_3(t) - x_5(t)] - 2ax_2(t) - a^2 x_1(t), \\ \dot{x}_3(t) = x_4(t), \\ \dot{x}_4(t) = Aa\{p(t) + C_2 S[C_1 x_1(t)]\} - 2ax_4(t) - a^2 x_3(t), \\ \dot{x}_5(t) = x_6(t), \\ \dot{x}_6(t) = Bb\{C_4 S[C_3 x_1(t)]\} - 2bx_6(t) - b^2 x_5(t), \end{cases} \tag{7}$$

where $x_3(t) - x_5(t)$ is the output signal which denotes the average depolarization of pyramidal cells and is used to model the EEG signal.

The above single neural population model concentrates on the brain's dynamical behaviors of a separate area. The spatial characters of EEG signals cannot be simulated by such a model. It is appropriate for multiple coupled neural populations model (Figs. 1(b) and 1(c)) to model the spatial characters of EEG because it takes into account the interaction between two or more cortical areas through introducing parameters related to the ways of populations connected and the delays associated with this connections. In Fig. 1(b), population l is described concretely by Fig. 1(c). As is observed in Figs. 1(b) and 1(c), a gain constant K_{lj} is introduced to define

the strength of coupling between population l and population j while a filter with an impulse response $h_{\rm d}(t) = w(t)Aa_{\rm d}t\,{\rm e}^{-a_{\rm d}t}$ is introduced to model the delay of connections from population l, where $a_{\rm d}$ is average time delay on efferent connection from population l. Appropriate setting of K_{lj} allows the populations to be interconnected unidirectionally or bidirectionally. The function $h_{\rm d}(t)$ is able to be rewritten as the form of (6), where $G = A$ and $g = a_{\rm d}$. Therefore, multiple coupled neural populations model is described by a set of eight first-order ordinary differential equations per population

$$\begin{cases} \dot{x}_{1l}(t) = x_{2l}(t), \\ \dot{x}_{2l}(t) = AaS[x_{3l}(t) - x_{5l}(t)] - 2ax_{2l}(t) - a^2 x_{1l}(t), \\ \dot{x}_{3l}(t) = x_{4l}(t), \\ \dot{x}_{4l}(t) = Aa\{p_l(t) + C_2 S[C_1 x_{1l}(t)] + \sum\limits_{j=1,2,\ldots,N, j\neq l} K_{lj} \\ \qquad \times x_{7j}(t)\} - 2ax_{4l}(t) - a^2 x_{3l}(t), \\ \dot{x}_{5l}(t) = x_{6l}(t), \\ \dot{x}_{6l}(t) = BbC_4 S[C_3 x_{1l}(t)] - 2bx_{6l}(t) - b^2 x_{5l}(t), \\ \dot{x}_{7l}(t) = x_{8l}(t), \\ \dot{x}_{8l}(t) = Aa_{\rm d} S[x_{3l}(t) - x_{5l}(t)] - 2a_{\rm d} x_{8l}(t) - a_{\rm d}^2 x_{7l}(t), \end{cases} \tag{8}$$

where the subscript l $(l = 1, 2, \ldots, N)$ represents the population under consideration, population l receives afferent information from population j $(j = 1, 2, \ldots, N,\ j \neq l)$ and the neighborhood $(p_l(t))$, $x_{3l}(t) - x_{5l}(t)$ is the output of population l and is assumed to model the EEG signal. All parameters in Fig. 1 are set on a physiological interpretation basis. The standard value of the parameters is given anatomically as

$$\begin{aligned} &A = 3.25\ {\rm mV}, \quad B = 22\ {\rm mV}, \quad a = 100\ {\rm s}^{-1}, \quad b = 50{\rm s}^{-1}, \\ &v_0 = 6\ {\rm mV}, \quad e_0 = 2.5\ {\rm s}^{-1}, \quad r = 0.56\ {\rm mV}^{-1}, \quad a_{\rm d} = 33\ {\rm s}^{-1}, \\ &C_1 = 135, \quad C_2 = 108, \quad C_3 = 33.75, \quad C_4 = 33.75. \end{aligned} \tag{9}$$

The details on how these values are obtained can be found in Ref. [9]. Each population in Eq. (8) produces well-defined alpha activity under standard parameters. However, a modification of parameters may result in the generation of epileptiform spikes as shown in simulation section.

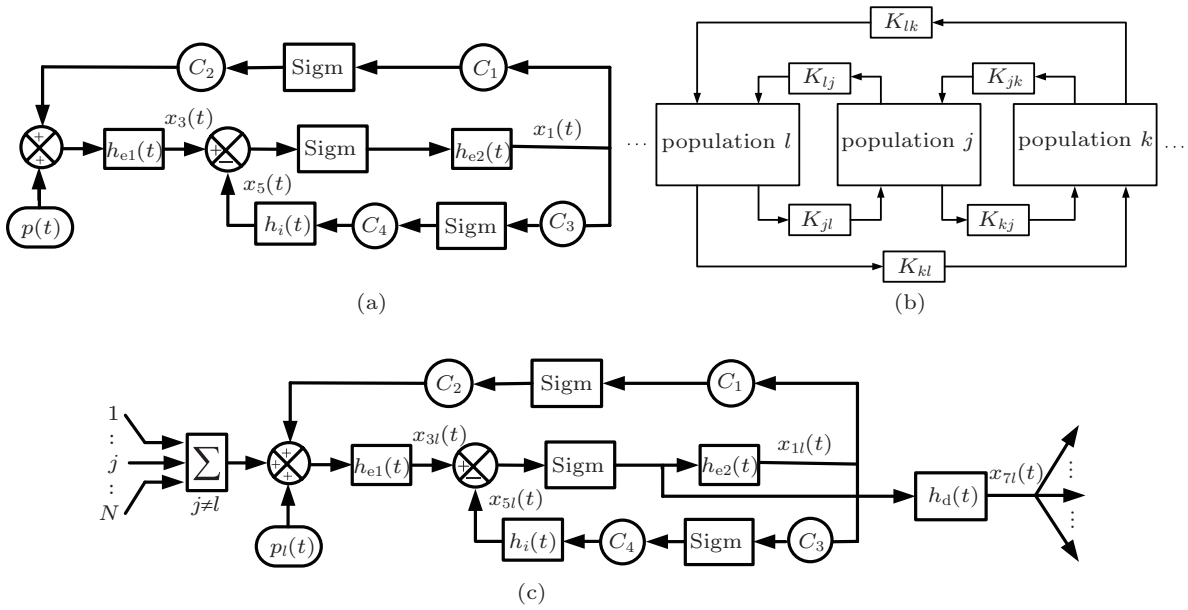


Fig. 1. (color online) Structure of the neural mass model. (a) Single neural population model. (b) Multiple coupled neural populations model. (c) Elementary model for a given population l.

3. UKF control of epileptiform spikes

Since the neural mass model is highly nonlinear, it is appropriate to employ the UKF as an observer to calculate a control signal for controlling epileptiform spikes in the model.

Given a nonlinear relationship $\boldsymbol{x}_{i+1} = \boldsymbol{F}x_i$, where $\boldsymbol{F}$ represents one-step dynamics of a system. The observation of the system is described by a function $\boldsymbol{G}$ which is contaminated by noise with covariance matrix $\boldsymbol{R}$. For a D_x-dimensional normally distributed random variable $\boldsymbol{x}$, its mean and covariance matrix are stored in $2D_x$ sigma points $\mathcal{X}_1, \ldots, \mathcal{X}_{2D_x}$, denoting the D_x columns of the matrix $\bar{\boldsymbol{x}} + \sqrt{D_x \boldsymbol{P}}$ together with the D_x columns of the matrix $\bar{\boldsymbol{x}} - \sqrt{D_x \boldsymbol{P}}$, where $\boldsymbol{P}$ is the covariance matrix for the errors in $\boldsymbol{x}$, $\sqrt{\cdot}$ indicates the matrix square root and $\bar{\boldsymbol{x}}$ is set as the mean of the distribution. Using one-step dynamics $\boldsymbol{F} : D_x \to D_x$ to sigma points, $\tilde{\boldsymbol{X}}_n = \boldsymbol{F}(\mathcal{X}_n)$ $(n = 1, 2, \ldots, 2D_x)$ is followed. Observation of the new states is $\tilde{\boldsymbol{Y}}_n = \boldsymbol{G}(\tilde{\boldsymbol{X}}_n)$ $(n = 1, 2, \ldots, 2D_x)$. A priori state estimate and a priori measurement estimate are defined as

$$\tilde{\boldsymbol{x}} = \frac{1}{2D_x} \sum_{n=1}^{2D_x} \tilde{\boldsymbol{X}}_n, \quad \tilde{\boldsymbol{y}} = \frac{1}{2D_x} \sum_{n=1}^{2D_x} \tilde{\boldsymbol{Y}}_n. \tag{10}$$

Then, priori covariance is defined as

$$\tilde{\boldsymbol{P}}_{xx} = \frac{1}{2D_x}\sum_{n=1}^{2D_x}(\tilde{\boldsymbol{X}}_n - \tilde{\boldsymbol{x}})(\tilde{\boldsymbol{X}}_n - \tilde{\boldsymbol{x}})^{\mathrm{T}}, \tag{11}$$

$$\tilde{\boldsymbol{P}}_{xy} = \frac{1}{2D_x}\sum_{n=1}^{2D_x}(\tilde{\boldsymbol{X}}_n - \tilde{\boldsymbol{x}})(\tilde{\boldsymbol{Y}}_n - \tilde{\boldsymbol{y}})^{\mathrm{T}}, \tag{12}$$

$$\tilde{\boldsymbol{P}}_{yy} = \frac{1}{2D_x}\sum_{n=1}^{2D_x}(\tilde{\boldsymbol{Y}}_n - \tilde{\boldsymbol{y}})(\tilde{\boldsymbol{Y}}_n - \tilde{\boldsymbol{y}})^{\mathrm{T}} + \boldsymbol{R}. \tag{13}$$

The Kalman gain matrix is denoted as $\boldsymbol{K} = \tilde{\boldsymbol{P}}_{xx}\tilde{\boldsymbol{P}}_{yy}^{-1}$. By the a posteriori quantities, the Kalman estimate of the state and the covariance matrix of the state estimate are given by

$$\hat{\boldsymbol{x}} = \tilde{\boldsymbol{x}} + \boldsymbol{K}(\boldsymbol{y} - \tilde{\boldsymbol{y}}), \quad \hat{\boldsymbol{P}}_{xx} = \tilde{\boldsymbol{P}}_{xx} - \boldsymbol{K}\tilde{\boldsymbol{P}}_{xy}^{\mathrm{T}}, \tag{14}$$

where $\boldsymbol{y}$ is the actual observation. Using the observation function again, a posteriori version of the observation variable $\hat{\boldsymbol{y}} = \boldsymbol{G}(\hat{\boldsymbol{x}})$ is derived.

In what follows, a UKF control strategy is proposed to control epileptiform spikes in the neural mass model, as shown in Fig. 2. In this context, 'control' indicates that turning the high-amplitude epileptiform spikes into the signal that reflects the normal activities. In Fig. 2, $\boldsymbol{F}$ and $\boldsymbol{G}$ represent the dynamical system and the observation function respectively, η is the normal distribution of random noise which is added to the output of the model to create the noise-contaminated observable output $\boldsymbol{y}_i$, $\boldsymbol{L}$ represents the control gain matrix, $\hat{\boldsymbol{y}}_i$ is the corresponding estimate of observable output, $\boldsymbol{u}_i$ is the control law which is constructed by the estimation of observable output $\hat{\boldsymbol{y}}_i$ from the UKF observer.

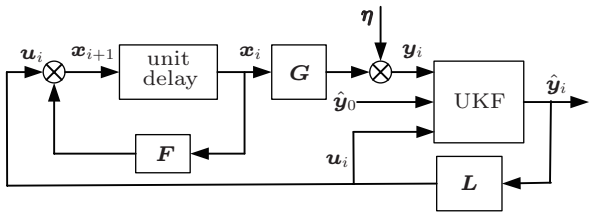


Fig. 2. The UKF control strategy for controlling epileptiform spikes in the neural mass model.

4. Simulation results

In this section, several numerical simulations are provided to validate the possibility of the neural mass model to produce epileptiform spikes and illustrate the effectiveness of proposed model-based UKF control strategy.

4.1. Epileptiform spikes in the neural mass model

For the past decades, mechanisms of epileptic seizures have been studied widely. Some work demonstrated that interictal or ictal spike discharges in the EEG in focal or partial seizures are due to an area of the cortex that is excessively excitable.[26] Other work showed that the interactions between neural populations are strengthened during epilepsy seizures.[27] In what follows, the neural mass model is demonstrated to be able to produce epileptiform spikes and the causality relations of the produced signals among underlying populations is clarified by numerical simulations. A fourth-order Runge–Kutta differential solver is used to solve Eqs. (7) and (8) in simulations.

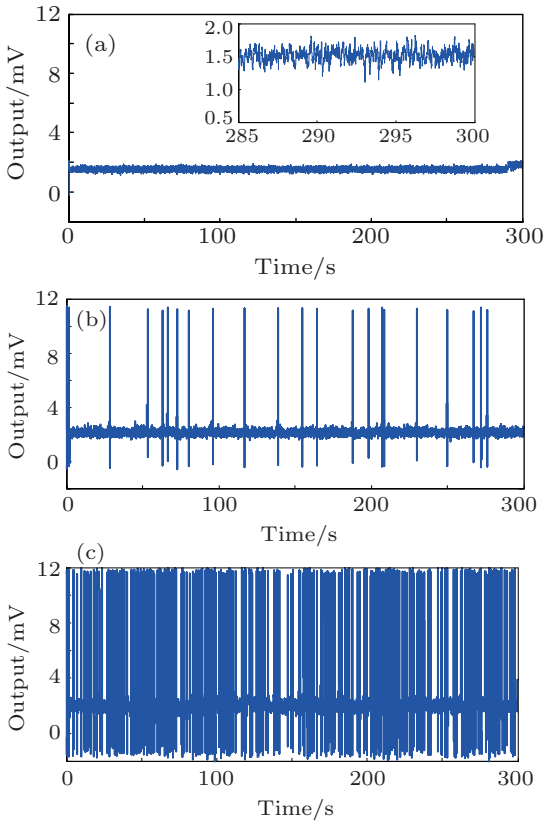


Fig. 3. (color online) Simulated signals of the single neural population model. Starting from a normal activity (a), the progressive increase of the average excitatory gain A makes the model produce sporadic (b) and frequent (c) spikes.

First, the single neural population model represented as Eq. (7) is considered. The input $p(t)$ is assumed to be a Gaussian white noise. The simulated signals with different values of A is presented in Fig. 3. The output of Eq. (7) with standard parameters is shown in Fig. 3(a). An inset is given to show the zoom-in data. The waveform resembles the spontaneous EEG recorded from neocortical structure electrodes during interical periods.[9] Thus, it reflects a normal activity resembling that reflected by real stereo-electroencephalographic (SEEG) signals. When A is increased to 3.4 mV or 3.6 mV and residual parameters keep standard, the output exhibits sporadic spikes (Fig. 3(b)) or frequent spikes (Fig. 3(c)). These aberrant dynamics strongly resemble real SEEG signals recorded before and during a seizure from a neocortical mid temporal gyrus.[9] Based on these results, it is indicated that the emergence of epileptiform spikes is caused by the divergence of A from the standard value and the average frequency of rhythmic discharge of spikes increases as the value of A increases.

For the underlying model, A and B determine the amplitude of the excitatory and inhibitory post-synaptic potential, respectively. In other words, the excitation/inhibition ratio A/B is related to the balance between excitatory and inhibitory processes. If A is increased from the standard value, the value of A/B is increased, which makes the underlying neural population hyperexcitable and subsequently results in the emergence of epileptiform spikes. Thus, the value of A/B influences the type of intra-population dynamics generated by the model.

Then a regular network represented as Eq. (8) with three identical neural populations (Fig. 4) is considered. The input $p_l(t)$ is assumed to be a Gaussian white noise. Population 1 is made hyperexcitable by setting $A = 3.4$ mV and keeping residual parameters standard. Populations 2 and 3 exhibit normal activity by keeping all parameters standard. Figure 5 shows the simulated dynamics of the model with different values of coupling constants. When $K_{21} = K_{32} = K_{13} = 0$, population 1 produces sporadic spikes appearing randomly while populations 2 and 3 produce signals reflecting normal activities (Figs. 5(a)–5(c)). When $K_{21} = 90$, $K_{32} = 100$, and $K_{13} = 0$, the propagation of sporadic spikes from population 1 to populations 2 and 3 is observed, as shown in Figs. 5(d)–5(f). It is conjectured that sporadic spikes in populations 2 and 3 are due to those in population 1 and the increase of the coupling constants K_{21} and K_{32}. When $K_{21} = K_{32} = K_{13} = 100$, a simulated EEG series with spikes resembling real EEG signals during the propagation of temporal lobe seizure[9] is observed, as shown in Figs. 5(g)–5(i). The introduction of K_{13} results in the generation of sustained spike discharges. For the underlying model, K_{lj} is used to alter the strength or direction of interactions between population l and population j. Thus, the conclusion is drawn from above analysis that the coupling strength and the coupling direction control the causality relations of the produced signals among the underlying populations.

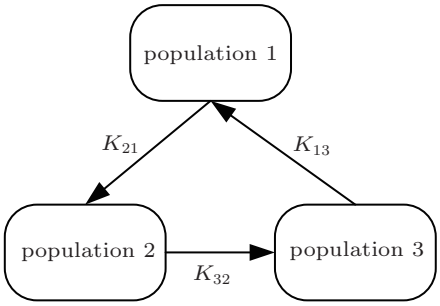


Fig. 4. A regular network of three coupled neural populations.

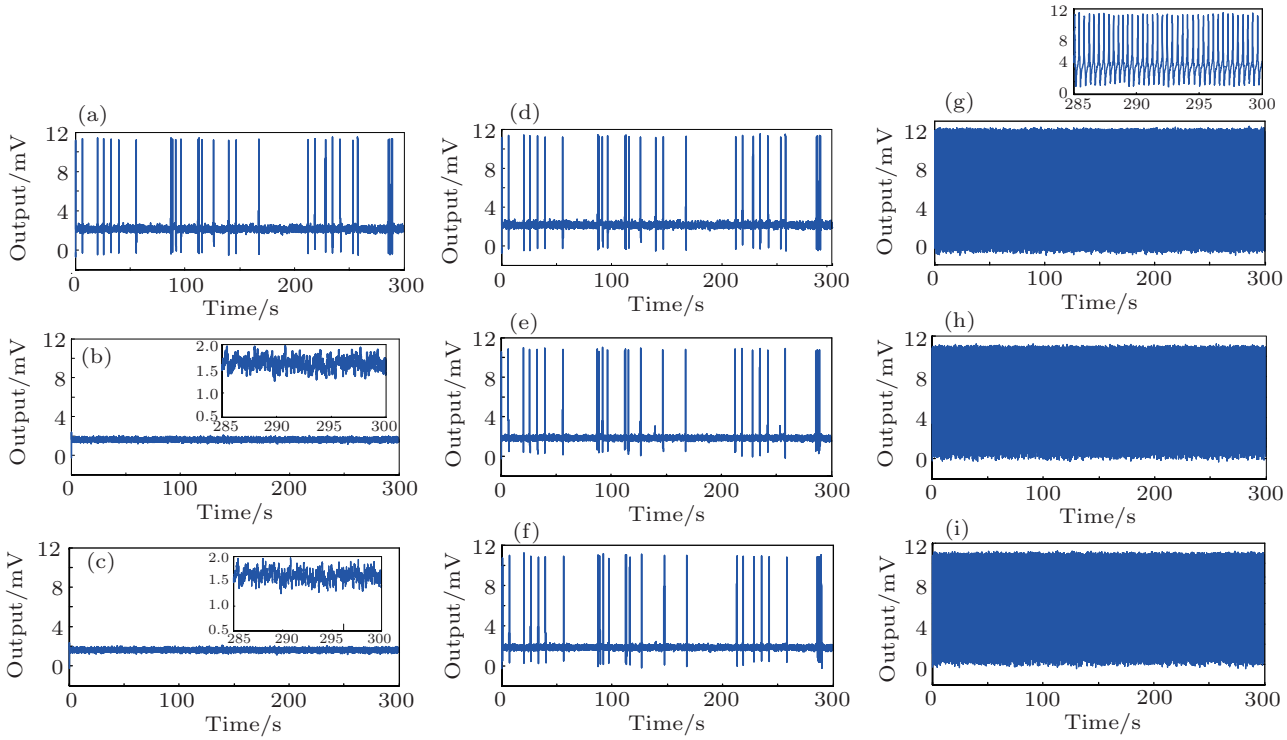


Fig. 5. (color online) Simulated signals of the regular network of three coupled neural populations with different coupling constants. (a)–(c) $K_{21} = K_{32} = K_{13} = 0$. (d)–(f) $K_{21} = 90$, $K_{32} = 100$, $K_{13} = 0$. (g)–(i) $K_{21} = K_{32} = K_{13} = 100$.

4.2. Control of epileptiform spikes

In this subsection, the strategy given in Fig. 2 is implemented to control epileptiform spikes in the neural mass model. Simulations are provided to show the effectiveness of the underlying control strategy. In order to demonstrate the role that the UKF plays, a direct proportional feedback control

with a control law constructed directly by the noisy measured data ($\boldsymbol{u}_i = \boldsymbol{L}\boldsymbol{y}_i$) is also used to control the epileptiform spikes in the neural mass model.

For the single neural population model represented by Eq. (7), the control gain matrix $\boldsymbol{L}$ is chosen as

$$\boldsymbol{L} = \begin{pmatrix} 0 & 0 & 0 & \bar{L} & 0 & 0 \end{pmatrix}^{\mathrm{T}} \tag{15}$$

where $\bar{L}$ is a constant number. The output (Fig. 6) and the total control energy (Table 1) are recorded for different values of $\bar{L}$ and A. When $A = 3.4$ mV, the output with the application of direct proportional feedback control and UKF control $\bar{L} = -0.1215$ is presented in Figs. 6(a) and 6(b). It is illustrated that the former control strategy substantially reduces the number of sporadic spikes by comparing Figs. 3(b) and 6(a), while the latter one suppresses all spikes. For a relatively high magnitude of gain ($\bar{L} = -0.18$), the spikes do not occur by using both control strategies. The output is omitted like Fig. 6(b). The total control energy needed in the UKF control is less than that of the proportional feedback control, as shown in Table 1. When $A = 3.6$ mV, the output of the model controlled by the two control strategies with $\bar{L} = -0.502$ is shown in Figs. 6(c) and 6(d). Similarly, the application of the direct proportional feedback control substantially reduces the number of frequent spikes (comparing Figs. 3(c) and 6(c)), but the use of the UKF control suppresses all spikes (Fig. 6(d)). For higher magnitude of gain level ($\bar{L} = -0.65$), the spikes are suppressed by using both control schemes. The output in this case is omitted because it is similar to Fig. 6(d). The UKF control needs less total control energy in feedback than the proportional feedback control (Table 1).

Table 1. The total control energy needed in the direct proportional feedback control and the UKF control (single neural population model, $t = 300$ s).

A/mV	$\bar{L}$	Total control energy/mV^2	
		Direct proportional feedback control	UKF control
3.4	–0.1215	27477.45	21565.69
3.4	–0.18	56878.22	45721.88
3.6	–0.502	482023.74	301210.34
3.6	–0.65	464171.77	423182.61

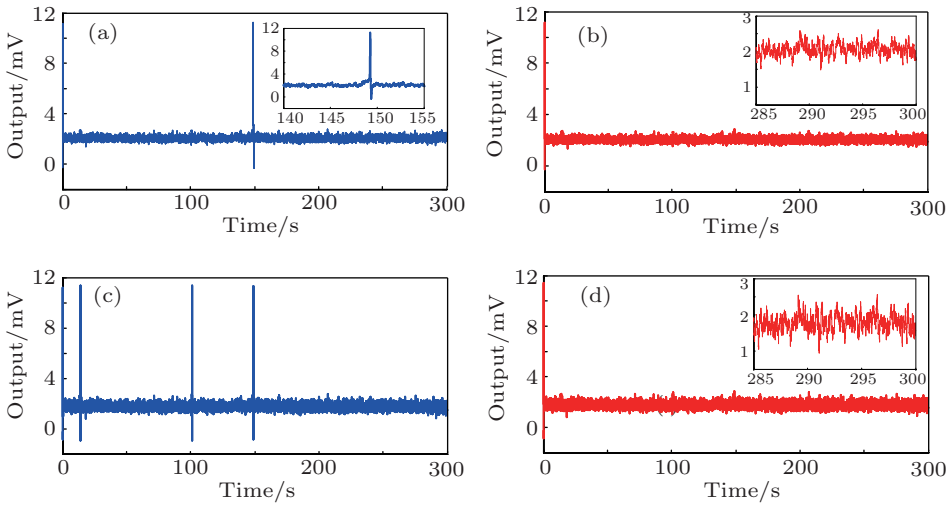


Fig. 6. (color online) The output with the use of the direct proportional feedback control (blue traces) and the UKF control (red traces) to the single neural population model. (a)–(b) $A = 3.4$ mV and $\bar{L} = -0.1215$. (c)–(d) $A = 3.6$ mV and $\bar{L} = -0.502$.

For the regular network represented by Eq. (8) with three coupled neural populations, $\boldsymbol{L}$ is set as

$$\boldsymbol{L} = \begin{pmatrix} \tilde{\boldsymbol{L}} & 0_{3\times 8} & 0_{3\times 8} \end{pmatrix}^{\mathrm{T}}, \tag{16}$$

where

$$\tilde{\boldsymbol{L}} = \begin{pmatrix} 0 & 0 & 0 & \bar{L} & 0 & 0 & 0 & 0 \\ 0 & 0 & 0 & 0 & 0 & 0 & 0 & 0 \\ 0 & 0 & 0 & 0 & 0 & 0 & 0 & 0 \end{pmatrix}, \tag{17}$$

$\bar{L}$ is a constant number, $\mathbf{0}_{3\times 8}$ is a 3×8 zero matrix. In the following analysis, population 1 is assumed to be hyperexcitable by keeping all parameters standard except for A, which is set as 3.4 mV. Populations 2 and 3 are assumed to exhibit normal activity by keeping all parameters standard. Thus, equation (16) implies the control action is imposed on the hyperexcitable population 1. The output (Fig. 7) and the total control energy (Table 2) are recorded for different values of $\bar{L}$, for different values of K_{lj}. When $K_{21} = 90$, $K_{32} = 100$, $K_{13} = 0$, the network is controlled by the direct proportional feedback control

and the UKF control with $\bar{L} = -0.127$, and the corresponding output of population 1 is presented in Figs. 7(a) and 7(b) (the output of populations 2 and 3 is not shown, which is similar to that of population 1). It is shown that the former control strategy substantially reduces the number of spikes whereas the latter one suppresses all spikes successfully. For a relatively high magnitude of gain ($\bar{L} = -0.2$), these sparse spikes do not occur under both control schemes. The output in this case is omitted because it is similar to Fig. 7(b). The total control energy in the UKF control is less than that of the proportional feedback control, as shown in Table 2. When $K_{21} = K_{32} = K_{13} = 100$, the output of the network controlled by the two control strategies with $\bar{L} = -0.865$ is shown in Figs. 7(c) and 7(d). Although the number of spikes reduces (please refer to the inset in Figs. 5(c) and 7(c)), sustained discharges of spikes still exist in the three neural populations by using the direct proportional feedback control. However, this abnormal discharge is eliminated and normal activities are derived by using the UKF control (Fig. 7(d)). For higher magnitude of gain level ($\bar{L} = -0.885$), sustained discharges of spikes do not occur under both control schemes but the UKF control needs less total control energy in feedback than the proportional feedback control, as shown in Table 2.

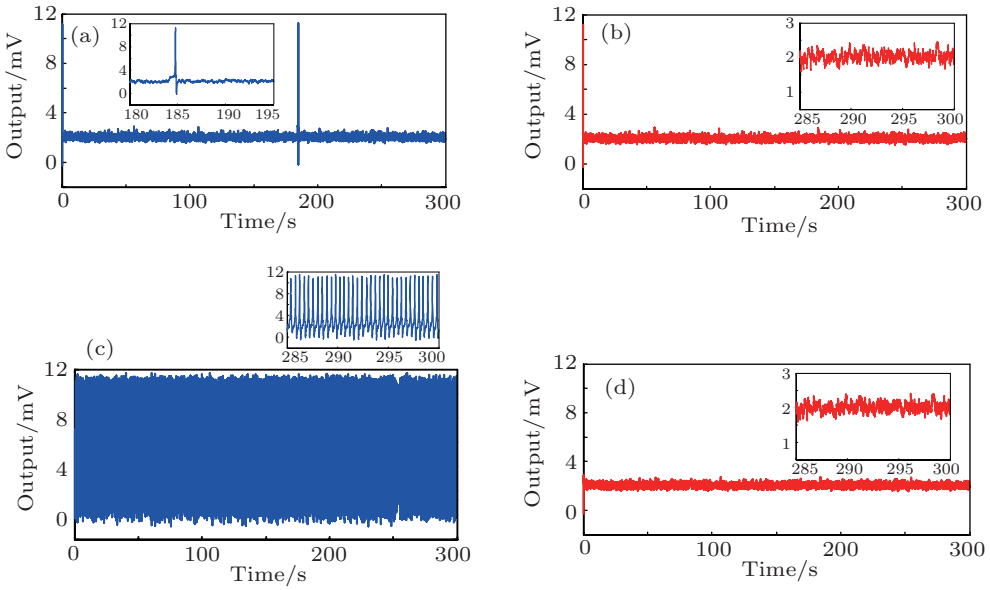


Fig. 7. (color online) The output of population 1 with the use of the direct proportional feedback control (blue traces) and the UKF control (red traces) to three coupled neural populations model. (a)–(b) $\bar{L} = -0.127$ and $K_{21} = 90$, $K_{32} = 100$, $K_{13} = 0$. (c)–(d) $\bar{L} = -0.865$ and $K_{21} = K_{32} = K_{13} = 100$.

Table 2. The total control energy needed in the direct proportional feedback control and the UKF control (three coupled neural populations model, $t = 300$ s).

Coupling constants	$\bar{L}$	Total control energy/mV^2	
		Direct proportional feedback control	UKF control
$K_{21} = 90$, $K_{32} = 100$	–0.127	29528.17	21425.75
$K_{21} = 90$, $K_{32} = 100$	–0.2	68602.60	58232.87
$K_{21} = K_{32} = K_{13} = 100$	–0.865	28948982.46	960245.30
$K_{21} = K_{32} = K_{13} = 100$	–0.885	1070318.91	995966.83

As we have expected, control of epileptiform spikes in the single neural population model can be reached by using the UKF control. The total control energy has a significant increase as the magnitude of A is increased. Control of epileptiform spikes in the network of multiple coupled neural populations can also be reached by using the UKF control as long as the control action is imposed on appropriate populations. The increase of coupling constant K_{lj} results in the increase of total control energy. The comparison between the UKF control and the direct proportional feedback control illustrates that the application of the UKF as an observer could make the total control energy reduce or the epileptiform spikes in the underlying model disappear completely and quickly.

5. Conclusion

We study the control problem of epileptiform spikes in the neural mass model by using the close-loop UKF control strategy. We show that epileptiform spikes in both the single neural population and the regular network of coupled populations can

be controlled by using the UKF control. The increase of the excitation/inhibition ratio and the coupling strength makes the total control energy increase. In comparison with the direct proportional feedback control, the application of the UKF can reduce the total control energy or let the epileptiform spikes in the underlying model disappear completely and quickly. This is owing to the filtering role that the UKF plays. In a word, it is feasible to apply the proposed strategy to control epileptiform EEG activity, which is simulated by the neural mass model. The application of the UKF observer can optimize the control performances like control energy comparing to the direct proportional feedback control.

The control strategy in this study provides a theoretical basis for the electrical stimulation treatment of epilepsy. We are tying to construct a real framework that can be used in future experiment applications. The strategy will be implemented through feedback electrical fields in an *in vivo* situation. There are various applications such as the control of Parkinson's disease for which the strategy might be applied. We hope it can play potential roles in human brain functional disorders disease therapy.

Acknowledgment

The authors would like to thank Prof. Steven J. Schiff and Dr. Logan Voss for their valuable suggestions.

References

[1] Li L, Jin Z L and Li B 2011 *Chin. Phys. B* **20** 038701
[2] Wang J and Zhao D Q 2012 *Chin. Phys. B* **21** 028703
[3] Andrzejak R G, Schindler K and Rummel C 2012 *Phys. Rev. E* **86** 046206
[4] Serge F T, Oleg Y P, Yuriy S P, Sergey A D and Alexander Y K 2012 *Physica A* **391** 1179
[5] Park C, Worth R M and Rubchinsky L L 2011 *Phys. Rev. E* **83** 042901
[6] David O and Friston K J 2003 *Neuroimage* **20** 1743
[7] Lopes da Silva F H, Hoeks A, Smits H and Zetterberg L H 1974 *Kybernetik* **15** 27
[8] Ursino M, Cona F and Zavaglia M 2010 *Neuroimage* **52** 1080
[9] Wendling F, Bellanger J J, Bartolomei F and Chauvel P 2000 *Biol. Cybern.* **83** 367
[10] Wendling F, Bartolomei F, Bellanger J J and Chauvel P 2002 *Eur. J. Neurosci.* **15** 1499
[11] Goodfellow M, Schindler K and Baier G 2011 *Neuroimage* **55** 920
[12] Rosenow F and Lüders H 2011 *Brain* **124** 1683
[13] Goodfellow M, Schindle K and Baier G 2012 *Neuroimage* **59** 2644
[14] Böex C, Vulliémoz S, Spinelli L, Pollo C and Seeck M 2007 *Seizure* **16** 664
[15] Sun F T, Morrell M J and Wharen R E 2008 *Neurotherapeutics* **5** 68
[16] Sunderam S, Gluckman B, Reato D and Bikson M 2010 *Epilepsy and Behavior* **17** 6
[17] Chong M, Postoyan R, Nešić D, Kuhlmann L and Varsavsky A 2012 *Automatica* **48** 2986
[18] Kalman R E 1960 *Trans. ASME D* **82** 35
[19] Anderson B D O and Moore J B 1979 *Optimal Filtering* (New Jersey: Prentice-Hall)
[20] Sitz A, Schwarz U, Kurths J and Voss H U 2002 *Phys. Rev. E* **66** 016210
[21] Sauer T D and Schiff S J 2009 *Phys. Rev. E* **79** 051909
[22] Zhang Z T and Zhang J S 2010 *Chin. Phys. B* **19** 104601
[23] Leng H Z and Song J Q 2013 *Chin. Phys. B* **22** 030505
[24] Schiff S J and Sauer T D 2008 *J. Neural Eng.* **5** 1
[25] Ullah G and Schiff S J 2009 *Phys. Rev. E* **79** 040901
[26] Dichter M A 1997 *Epilepsia* **38** S2
[27] Fish D R, Gloor P, Quesney F L and Oliver A 1993 *Brain* **116** 397